Linear Disturbance Amplification Over Blunted Flat Plates in High-Speed Flows

A. Scholten,[1] H. Goparaju,[2] D. Gaitonde,[2] P. Paredes,[3] M. Choudhari,[4] F. Li[4]

[1]North Carolina State University
[2]Ohio State University
[3]National Institute of Aerospace
[4]Computational AeroSciences Branch, NASA Langley Research Center

AIAA Aviation 2022, FD-14: Stability and Transition: Hypersonic III
June 28, 2022, Chicago, IL

Outline

Outline

Previous Experiments and DNS

- Geometry and flow conditions informed by experimental[1] and DNS[2] work
- Blunt flat plates with leading edge $R_n = 0.5$ mm and total length $l = 400$ mm
- $M_\infty = 4,\ Re = 25.3 \times 10^6$ m^{-1} $\rightarrow Re_n = 12650$
- Identified linear disturbances downstream when perturbations were introduced close to the nose, at entropy layer edge
- Comparison of density fluctuations at the entropy layer edge for (case 1) wall forcing, (case 2) BL forcing, (case 3) EL edge forcing.

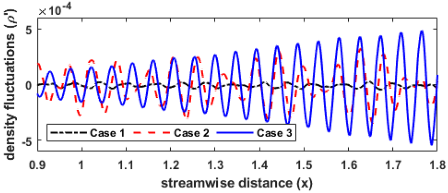

[1] V. Lysenko. "Influence of the entropy layer on the stability of a supersonic shock layer and transition of the laminar boundary layer to turbulence". In: Applied Mechanics and Technical Physics 31(06) (1990), 868 (5 pages).

[2] H. Goparaju and D. Gaitonde. Receptivity and instability of entropy-layer disturbances in blunted plate transition. AIAA 2021-2877. 2021. DOI: 10.2514/6.2021-2877.

Outline

1 Motivations

2 Computational Analysis
- Laminar Basic State Solution
- Modal Analysis
- Nonmodal Analysis
- Linear Forcing Analysis

3 Summary and Concluding Remarks

Computational Analysis

Laminar Basic State Solution

Laminar Basic State Solution

- VULCAN-CFD: shock-capturing, 2^{nd}-order finite-volume NS solver
- Shock-adapted grid with 1201×601 grid points
- $R_n = 0.05$, 0.5, and 2.5 mm; total length $l = 400$ mm
- $Re = 25.3 \times 10^6\ \text{m}^{-1}$, $T_0 = 290$ K, $T_w = 255.48$ K, Sutherland's law
- $Re_n = 1265$, 12650, and 63250

M_∞	u_∞ [m/s]	ρ_∞ [kg/m^3]	T_∞ [K]	$T_{\text{wall}}/T_{\text{wall,adiabatic}}$	P_0 [Pa]
4	666.32	0.1770	69.05	0.9959	5.3268×10^5
6	715.30	0.0744	35.37	1.0159	1.1926×10^6

- $M_\infty = 6$, $R_n = 0.05$ mm

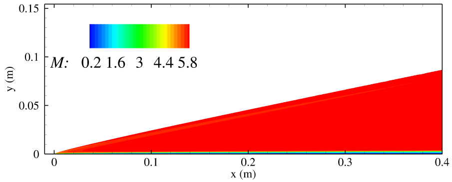

- $M_\infty = 6$, $R_n = 2.5$ mm

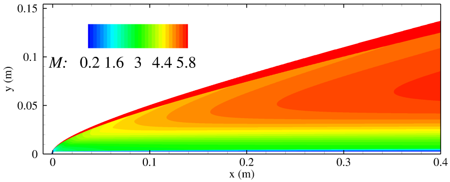

Axial Evolution

- Effect of leading edge bluntness and freestream conditions
- R_n = 0.05, 0.5, 2.5 mm; $M_\infty = 4$, $M_\infty = 6$
  - Boundary-layer thickness
  - Edge Mach number

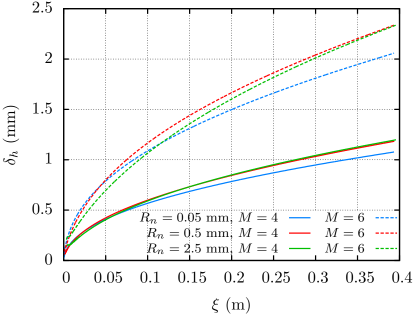

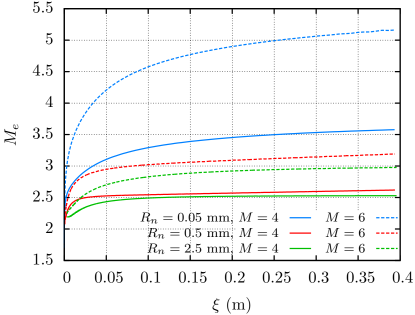

- Close to leading edge: δ_h decreases as R_n increases
- Downstream, $R_n = 0.05$ mm $\rightarrow R_n = 0.5$ mm: δ_h increases
- Increasing bluntness decreases M_e

Wall-Normal Profiles - Mach number

- $R_n = 0.05, 0.5, 2.5$ mm; $\underline{M_\infty = 4}$, $M_\infty = 6$ (dashed)

- $x = 0.08$ m
- $x = 0.18$ m
- $x = 0.28$ m

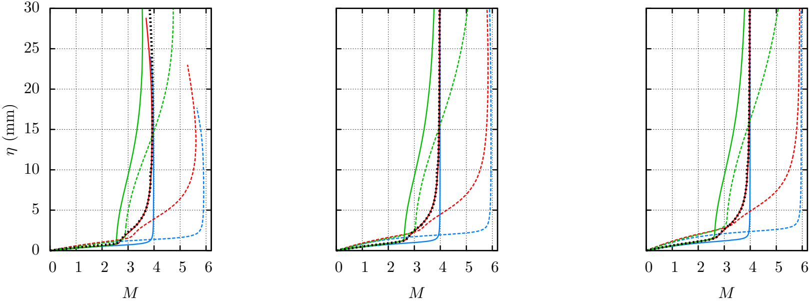

- Mach 4, $R_n = 0.5$ mm: matches **DNS**
- Mach 6, $x = 0.08$ m: nonmonotonic wall-normal gradients in Mach number above the boundary-layer edge $\rightarrow$ entropy layer effects
- Profiles are cutoff before the shock

Wall-Normal Profiles - Temperature

- $R_n = 0.05, 0.5, 2.5$ mm; $\underline{M_\infty = 4}$, $\underline{M_\infty = 6}$

- $x = 0.08$ m

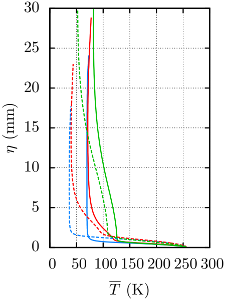

- $x = 0.18$ m

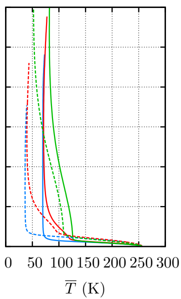

- $x = 0.28$ m

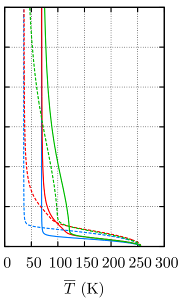

- Profiles eventually converge to freestream conditions
- Increasing bluntness increases temperature
- Increasing Mach number decreases temperature
- Profiles are cutoff before the shock

Computational Analysis

Modal Analysis

Linear Modal Analysis[3]

- Decomposition of flow variables:

$$\mathbf{q}(\xi,\eta,\zeta,t) = \bar{\mathbf{q}}(\xi,\eta) + \epsilon\tilde{\mathbf{q}}(\xi,\eta,\zeta,t); \quad \bar{\mathbf{q}} = \mathcal{O}(1); \quad \epsilon \ll 1$$

- Harmonic Linearized Navier-Stokes Equations (HLNSE):
  - exploit basic state independence w.r.t. time and spanwise direction
  - solution of a 2D linear system of equations

$$\tilde{\mathbf{q}}(\xi,\eta,\zeta,t) = \breve{\mathbf{q}}(\xi,\eta)\exp\left[\mathrm{i}\left(\beta\zeta - \omega t\right)\right]$$

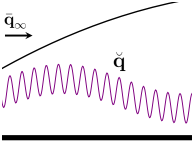

- **Parabolized Stability Equations (PSE):**
  - exploit slow variations in streamwise direction via separation of scales
  - parabolic integration in ξ coupled with normalization condition

$$\breve{\mathbf{q}}(\xi,\eta) = \hat{\mathbf{q}}(\xi,\eta)\theta(\xi);\ \theta(\xi) = \exp\left[\mathrm{i}\int_{\xi_0}^{\xi}\alpha(\xi')\,\mathrm{d}\xi'\right]$$

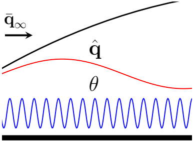

[3] P. Paredes et al. "Nosetip bluntness effects on transition at hypersonic speeds: experimental and numerical analysis". In: Journal of Spacecraft Rockets 56.2 (2019). DOI: 10.2514/1.A34277.

Linear Modal Analysis

- Mach 4, $\xi = 0.28$ m

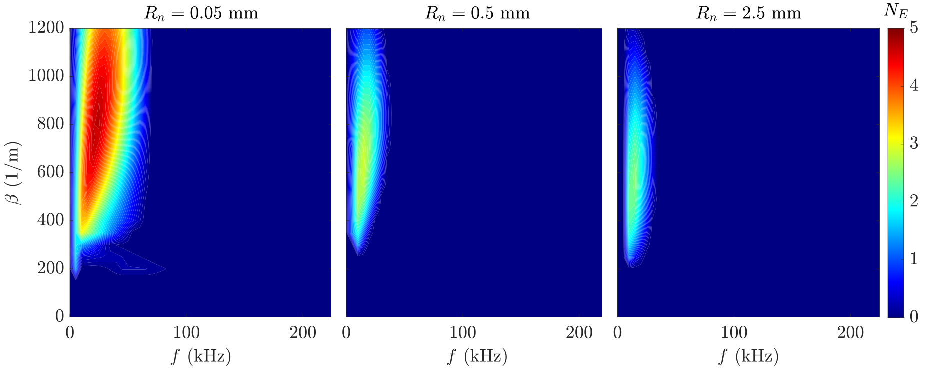

- Oblique disturbance, corresponding to Mack's first mode, is most amplified
- As the bluntness is increased, the disturbance: dampens, shifts to lower frequency, wavenumber decreases
  - Due to increased boundary-layer thickness influencing this boundary-layer disturbance

Linear Modal Analysis

- Mach 6, $\xi = 0.28$ m

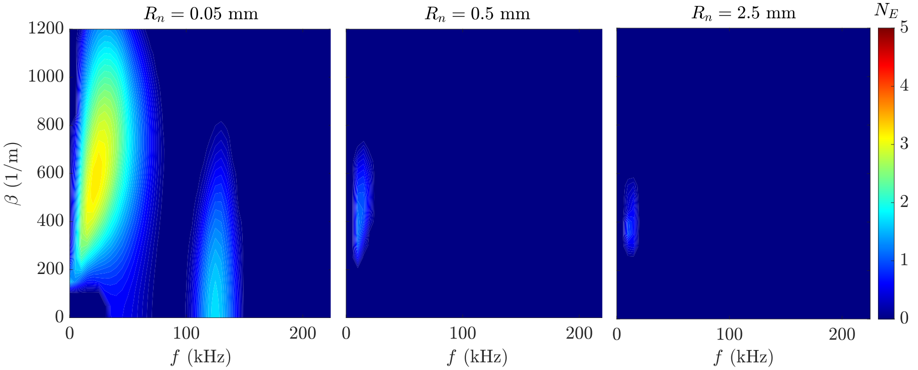

- Oblique disturbance, corresponding to Mack's first mode, is most amplified
- Weaker oblique disturbance than Mach 4
- Wavenumber associated with oblique disturbance decreases for higher M_∞
- Secondary, planar disturbance corresponding to Mack's second mode captured for $R_n = 0.05$ mm

Computational Analysis

Nonmodal Analysis

Linear Nonmodal or Inflow-Resolvent Analysis[4,5]

- Initial location selected close to the leading edge ($\xi_0 = 0.02$ m)
- Final location selected to match previous results ($\xi_1 = 0.28$ m)
- Optimal initial disturbance, $\tilde{\mathbf{q}}_0$: initial condition at ξ_0 that maximizes J:
  - Outlet energy gain: $J = G_E^{out} = \frac{E(\xi_1)}{E(\xi_0)}$
- Energy norm: $E(\xi) = \int_\eta \tilde{\mathbf{q}}(\xi)^* \mathbf{M}(\xi) \tilde{\mathbf{q}}(\xi)\, h_\xi\, h_\zeta\, \mathrm{d}\eta$

$$\mathbf{M}(\xi) = \mathrm{diag}\left[\frac{\bar{T}(\xi)}{\gamma\bar{\rho}(\xi)M^2}, \bar{\rho}(\xi), \bar{\rho}(\xi), \bar{\rho}(\xi), \frac{\bar{\rho}(\xi)}{\gamma(\gamma-1)\bar{T}(\xi)M^2}\right]$$

- Variational formulation using direct and adjoint **HLNSE**

$$\mathcal{L}(\tilde{\mathbf{q}}, \tilde{\mathbf{q}}^\dagger) = J(\tilde{\mathbf{q}}) - \langle \tilde{\mathbf{q}}^\dagger, \mathbf{L}\tilde{\mathbf{q}} \rangle$$

- Parametric analysis w.r.t. wavenumber (β) & frequency (f)

---

[4] P. Paredes et al. "Optimal growth in hypersonic boundary layers". In: AIAA Journal 54.10 (2016), pp. 3050–3061. DOI: 10.2514/1.J054912.

[5] P. Paredes et al. "Nosetip bluntness effects on transition at hypersonic speeds: experimental and numerical analysis". In: Journal of Spacecraft Rockets 56.2 (2019). DOI: 10.2514/1.A34277.

Nonmodal

- Mach 4, optimal disturbance energy gain over $\xi_0 = 0.02$ m to $\xi_1 = 0.28$ m

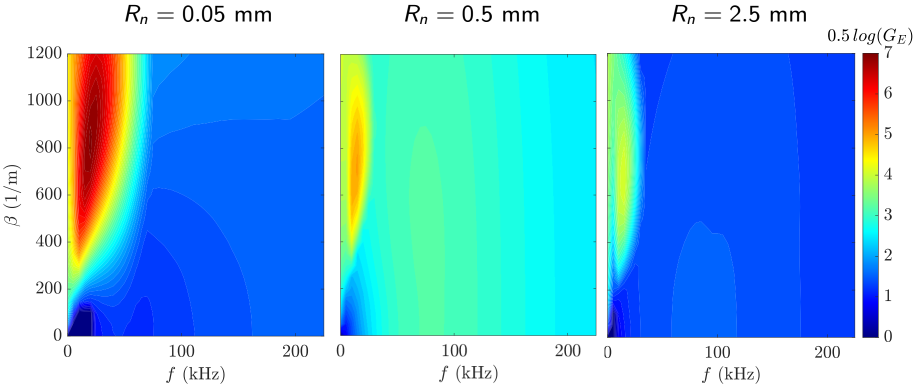

- Most unstable, oblique, mode location agrees with PSE
- Planar peak is identified at higher frequencies $80 \leq f \leq 120$ kHz
  - Non-monotonic increase with respect to R_n
- DNS with entropy layer edge forcing shows amplification of disturbances at $60 \leq f \leq 110$ kHz

Nonmodal

- Mach 6, optimal disturbance energy gain over $\xi_0 = 0.02$ m to $\xi_1 = 0.28$ m

$R_n = 0.05$ mm $\qquad R_n = 0.5$ mm $\qquad R_n = 2.5$ mm

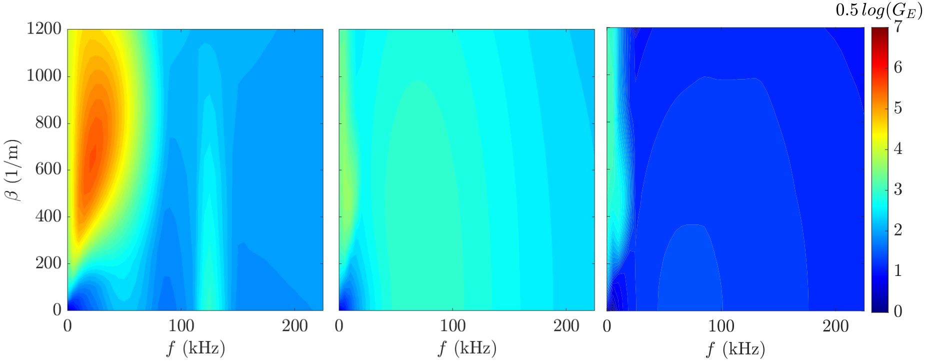

- Most unstable, oblique, mode location agrees with PSE
  - Secondary peak for $R_n = 0.05$ mm (Mack's second mode) also matches
- Planar peak is identified at higher frequencies $80 \leq f \leq 120$ kHz
  - Non-monotonic increase with respect to R_n
- $R_n = 0.5$ mm: both oblique and planar modes are comparable in amplitude

Contours of Flow Perturbations - Mach 4, $R_n = 0.5$ mm

- Nonmodal: $f = 66.6$ kHz, $\beta = 0$

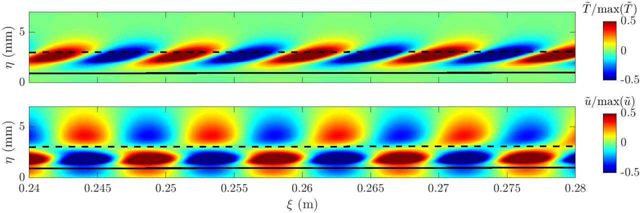

- DNS (Goparaju & Gaitonde, 2021): $f = 66.6$ kHz, $\beta = 0$, forcing at $x = 0.06$ m, δ_S with monopole width of 5 mm

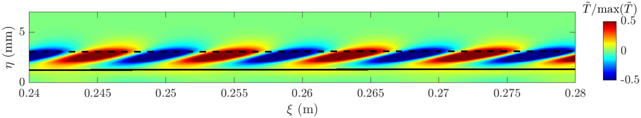

- **Nonmodal analysis and forced DNS capture the same entropy-layer disturbances**

Contours of Flow Perturbations - Mach 6, $R_n = 0.05$ mm

- Oblique: $f = 20$ kHz, $\beta = 650 \rightarrow$ Mack's first mode

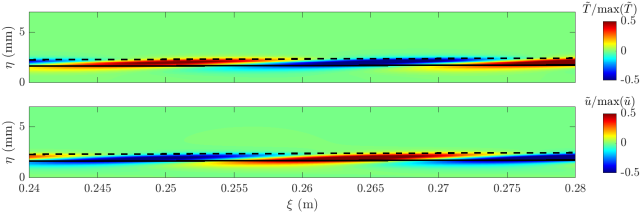

- Planar: $f = 125$ kHz, $\beta = 0 \rightarrow$ Mack's second mode

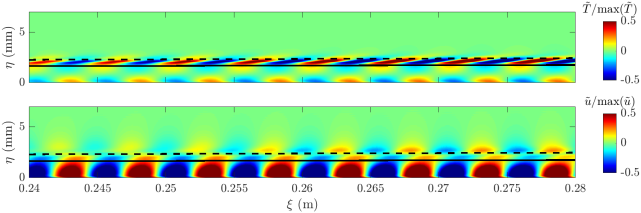

Contours of Flow Perturbations - Mach 6, $R_n = 2.5$ mm

- Planar: $f = 65$ kHz, $\beta = 0 \rightarrow$ entropy-layer disturbance

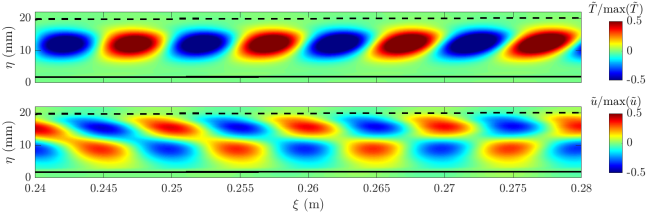

- Oblique: $f = 65$ kHz, $\beta = 450 \rightarrow$ entropy-layer disturbance

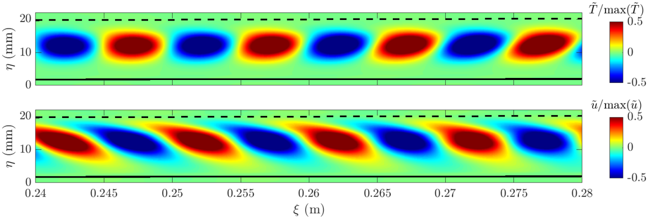

Computational Analysis

Linear Forcing Analysis

Linear Forcing Analysis

- Perturb streamwise velocity at $\xi_0 = 70$ mm for Mach 6, $R_n = 0.05$ and 2.5 mm
- Perturb at different wall-normal locations: on-wall, $\frac{1}{2}(\delta_h + \delta_S)$, δ_S
- Gaussian bump

$$g(\xi, \eta) = A \exp\left(-\frac{1}{2}\left(\frac{(\xi - \xi_0)^2}{\sigma_\xi^2} + \frac{(\eta - \eta_0)^2}{\sigma_\eta^2}\right)\right)$$

R_n, mm	δ_h, mm	δ_S, mm	ξ_0, mm	σ_ξ, mm	η_0, mm	σ_η, mm
0.05	0.9233	1.3951	70	1	0	1
			70	1	1.16	1
			70	1	1.38	1
2.5	0.8460	15.6	70	1	0	1
			70	1	8.26	1
			70	1	15.5	1

- Forced disturbance growth taken until $\xi_1 = 0.28$ m

Linear Forcing Analysis - Mach 6, $R_n = 0.05$ mm

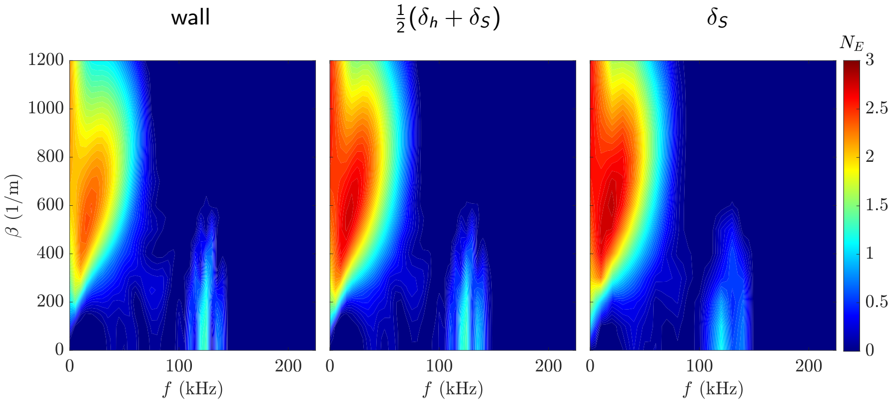

- Low-frequency streaks, oblique Mack's first mode, and planar Mack's second mode disturbances captured for all forcing locations
- Stronger oblique Mack's first mode as forcing is set further from the wall
- Entropy layer forcing yields weaker response of Mack's second mode disturbances

Linear Forcing Analysis - Mach 6, $R_n = 2.5$ mm

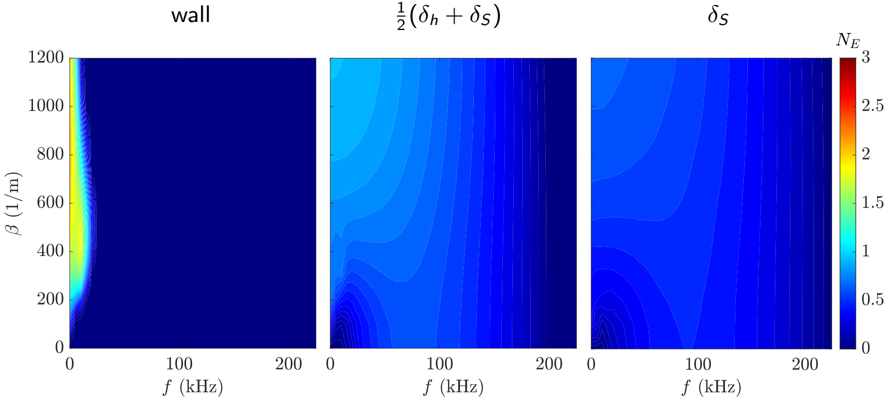

- Weak oblique Mack's first mode and weakens as forcing is set further from the wall
- Much weaker planar disturbances because Mack's second mode becomes stable for higher R_n
- Nonmodal entropy-layer disturbances excited only when forcing is above boundary-layer edge (in agreement with forced DNS)

Outline

Concluding Remarks

- PSE and HLNSE identifies Mack's first mode instability as most amplified for both flow conditions ($M_\infty = 4$ and 6)
- Mack's second mode instabilities captured at Mach 6 for $R_n = 0.05$ mm
- Broadband, nonmodal entropy-layer disturbances captured for $R_n = 0.5, 2.5$ mm
- Nonmodal analysis and forced DNS capture the same entropy-layer disturbances
- Linear forcing analysis at Mach 6:
  - $R_n = 0.05$ mm: low frequency streaks as well as Mack's first and second modes found for all forcing locations
  - $R_n = 2.5$ mm: wall forcing only induces oblique Mack's first mode and off-wall forcing induces entropy-layer diturbances
- By including receptivity effects with linear forcing analysis, narrower bands of perturbations are amplified based on the actuator location, shape, and dynamics
- Nonmodal analysis shown to be a useful and efficient technique to identify the complete disturbance spectrum in blunt hypersonic configurations

Thank You for Your Attention

- Acknowledgments
  - This research was sponsored in part by the U. S. Office of Naval Research (ONR) under award number N00014-20-1-2261 with P.O. Eric Marineau and by the NASA Hypersonic Technology Project (HTP) under the Aeronautics Research Mission Directorate (ARMD). Hemanth Goparaju is supported by the Office of Naval Research (Grant: N00014-21-1-2408) monitored by Dr. E. Marineau with R. Burnes as the technical point of contact.
  - Resources supporting this work were provided by the DoD High Performance Computing Modernization Program, the NASA High-End Computing (HEC) Program through the NASA Advanced Supercomputing (NAS) Division at Ames Research Center and the NASA K-Midrange Cluster at Langley Research Center.